Journal of Crystal Growth 378 (2013) 218–221

Contents lists available at SciVerse ScienceDirect

Journal of Crystal Growth

journal homepage: www.elsevier.com/locate/jcrysgro

Optical properties of $Zn_{1-x}Mn_xO$ thin films grown by molecular beam epitaxy

K.F. Chien [a], Y.L. Yang [a], A.J. Tzou [a], W.C. Chou [a,b,*]

[a] Department of Electrophysics, National Chiao Tung University, Hsin-Chu 30010, Taiwan
[b] NSC Taiwan Consortium of Emergent Crystalline Materials, Taiwan

ARTICLE INFO

Available online 4 December 2012

Keywords:
A3. Molecular beam epitaxy
B1. Oxides
B1. Zinc compounds
B2. Magneto-optic materials
B2. Semiconducting II–VI materials

ABSTRACT

$Zn_{1-x}Mn_xO$ ($x=0$–0.061) thin films were grown by molecular beam epitaxy (MBE) system. Transmittance shows an increase of the band gap with the increasing Mn concentration. Resonant Raman scattering (RRS) spectra showed 11 longitudinal optical phonon lines for the $Zn_{1-x}Mn_xO$ samples. For the $Zn_{0.997}Mn_{0.003}O$ sample, circular polarization degree of 9% was observed at magnetic field $B=5$ T. The dependence of circular polarization rate on the magnetic field intensity exhibits Brillouin type para-magnetism.

1. Introduction

$Zn_{1-x}Mn_xO$ was theoretically predicted [1] and experimentally observed [2] to exhibit ferromagnetism at room temperature. Spin dependent tunneling properties were observed in the metal-oxide-semiconductor diode consisting of ferromagnetic $Zn_{1-x}Mn_xO$ nanocrystals [3]. However, there was no ferromagnetism observed for the $Zn_{1-x}Mn_xO$ thin films grown by pulsed laser ablation and rf magnetron sputtering methods [4]. Mixed magnetic phases (paramagnetic and ferromagnetic) were reported for the $Zn_{1-x}Mn_xO$ nanostructures synthesized by chemical vapor deposition [5]. This controversy of paramagnetism or ferromagnetism in $Zn_{1-x}Mn_xO$ motivates intensive studies of magnetism in ZnO related materials in recent years [6,7]. In this study, $Zn_{1-x}Mn_xO$ thin films were grown by plasma-assisted MBE. The magneto-optical properties were investigated to study the magnetism of $Zn_{1-x}Mn_xO$ thin films and to explore the potential application of this material in the spintronic devices.

2. Experiments

$Zn_{1-x}Mn_xO$ thin film was grown on *c*-plane Al_2O_3 substrate by a SVT Associates MBE system equipped with conventional effusion cells for evaporation of elemental Zn (6*N*), Mg (6*N*), and Mn (5*N*). Oxygen (5*N*5) flow rate of 0.6 SCCM with plasma power 250 W is supplied via a rf-plasma source after additional gas purification. The substrates were degreased in acetone, methanol, and then chemically etched in H_2SO_4:H_3PO_4=3:1 at 160 °C for 15 min followed by deionized water rinse and spin drying. Before growth, the substrates were desorbed at 850 °C and treated in oxygen plasma, which is expected to produce an oxygen terminated Al_2O_3 surface. In order to reduce the lattice mismatch, MgO was grown at 650 °C as a buffer layer. Because the lattice misfit between the MgO and Al_2O_3 is 8%, that is lower than that between ZnO and Al_2O_3 (18%) [8]. A 325 nm He–Cd laser was used as the excitation source to obtain the PL and RRS spectra and a 800 W xenon lamp was the light source for the transmittance measurements. The RRS, PL and transmittance spectra were analyzed using a 0.55 m single-grating spectrometer and photomultiplier tube.

3. Results and discussion

Fig. 1(a) shows room temperature transmittance spectra of $Zn_{1-x}Mn_xO$ thin films with Mn concentration $x=0$, 0.009, 0.030 and 0.061. The absorption edge energy increasing with Mn concentration can be observed. Fig. 1(b) shows the absorption edge energy of the $Zn_{1-x}Mn_xO$ versus Mn concentration. The blue shift of the absorption energy is due to MnO having a larger band gap than ZnO [9]. The shift of the absorption edge can be expressed by the following equation.

$$E(x) = 3.337 + 3.056x\ (eV) \quad (1)$$

The experimental results are in good agreement with reference [9]. Furthermore, the broadening of the absorption edge increases with the Mn concentration. The broadening is mainly due to the increasing disorder with increasing Mn concentration in $Zn_{1-x}Mn_xO$. There are also obvious mid-gap absorption around 3 eV for higher

* Corresponding author at: Department of Electrophysics, National Chiao Tung University, Hsin-Chu 30010, Taiwan. Tel.: +886 3 571 2121; fax: +886 3 572 5230.
E-mail address: wuchingchou@mail.nctu.edu.tw (W.C. Chou).

0022-0248/$ - see front matter © 2012 Elsevier B.V. All rights reserved.
http://dx.doi.org/10.1016/j.jcrysgro.2012.11.052

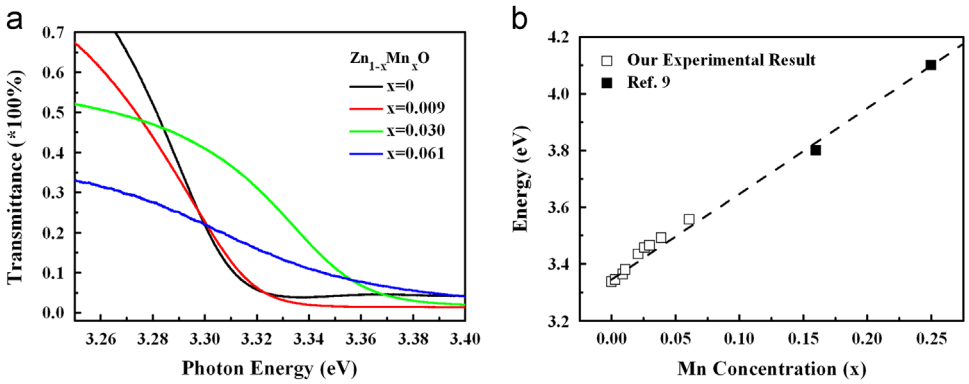

Fig. 1. (a) Room temperature transmittance spectra of $Zn_{1-x}Mn_xO$ thin films with Mn concentration $x=0$, 0.009, 0.030 and 0.061. (b) The absorption edge energy of $Zn_{1-x}Mn_xO$ thin films as a function of the Mn concentrations (x). The experimental results of ours (□) and reference [9] (■) are plotted.

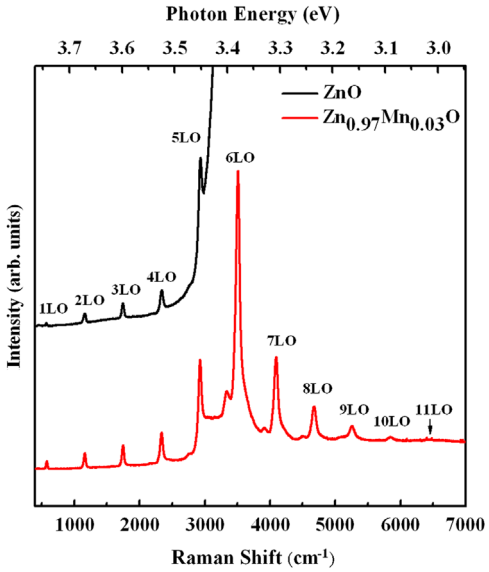

Fig. 2. Resonant Raman scatterings of ZnO and $Zn_{0.97}Mn_{0.03}O$ thin films, using the He–Cd laser ($\lambda=325$ nm).

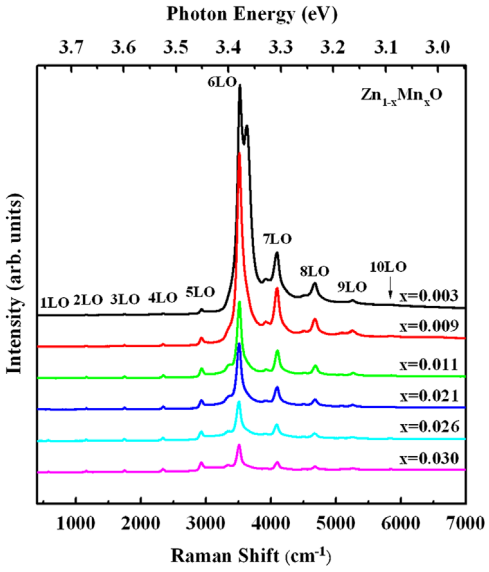

Fig. 3. Resonant Raman scatterings of $Zn_{1-x}Mn_xO$ thin films, using the He–Cd laser ($\lambda=325$ nm).

Mn concentration samples. This effect has been ascribed to the d–d transitions of the Mn^{2+} ion [10].

Fig. 2 shows low temperature (10 K) resonant Raman scattering (RRS) spectra of ZnO and $Zn_{0.97}Mn_{0.03}O$ thin films with the He–Cd laser ($\lambda=325$ nm) excitation. RRS experiment is performed under the excitation laser energy higher than the band gap, and the incident photon energy will be in resonance with the electronic interband transition. The peak at 578 cm^{-1} is the first-order longitudinal optical (LO) phonon mode [11], in which both O and Zn atoms vibrate in the same direction. The weak peak around 457 cm^{-1} is ascribed to the E_2 (high) mode. Compared with 440 cm^{-1} in bulk ZnO single crystal [11], the frequency of the E_2 (high) mode in our sample is slightly larger, it is mainly due to strain effect in the thin film. Under RRS condition, some intense peaks at frequency positions of approximately integer times 578 cm^{-1} contribute to the nth-order LO phonon scattering processes. These are intense LO phonon lines because of the Frohlich interaction, which is the interaction between electrons and the longitudinal electrical field induced by the LO phonons [12]. In addition, there are also some relatively weak peaks at frequency positions next to these LO phonon modes. Interestingly, the intervals of these weak peaks are also close to the frequency of LO phonon mode. Considering the frequency positions of these peaks, they are probably caused by the combination of E_2 (high) mode and multiple LO phonon scattering.

From the RRS spectra, we find 5 and 11 LO phonon modes for ZnO and $Zn_{0.97}Mn_{0.03}O$ samples, respectively. In previous studies [13], Scott et al. reported that the LO phonon numbers (n) in RRS spectra varies proportionally with the electron–phonon coupling coefficient (α), which is given as the ratio of the Frohlich interaction energy to the LO phonon energy. They also predicted the number of LO phonon modes in ZnO is more than $n=9$ in CdS. However, they only found $n=8$ in their ZnO sample. From our results, we could not find LO phonon lines for $n>5$ in ZnO due to the strong near band edge PL emission. However, for $Zn_{0.97}Mn_{0.03}O$, the near band edge emission is weak and due to the large electron–phonon coupling coefficient $\alpha=0.9$ (is assumed to be the same as ZnO), the observation of large amount of LO phonon lines ($n=11$) in RRS spectra can be understood.

Fig. 3 shows the RRS spectra of $Zn_{1-x}Mn_xO$ ($x=0.003$–0.030) thin films. Besides some intense LO phonon lines, there is an extra peak at 3632 cm^{-1} for $Zn_{0.997}Mn_{0.003}O$ sample. This peak is ascribed to the neutral donor bound exciton (D^0X) emission. As shown in the spectra, the LO phonon mode intensity at the frequency position of around 3500 cm^{-1}, which is assigned to the sixth-order LO phonon mode, is always the largest in each of

$Zn_{1-x}Mn_xO$ samples, and the intensity decreases with increasing Mn concentration. The behavior of intensity variation is mainly related to the band gap position, and it can be explained by using the Raman cross section for the nth-order LO phonon mode which is given as [14]

$$\sigma_n(\omega)=\mu^4\sum_{j=0}^{\infty}\left|\sum_{m=0}^{\infty}\frac{\langle g,n+j|e,m\rangle\langle e,m|g,j\rangle}{E_{ex}+(m-j)\hbar\omega_{LO}-\hbar\omega_i+i\hbar\Gamma}\right|^2 exp\left(-\frac{j\hbar\omega_{LO}}{k_BT}\right) \quad (2)$$

where μ is the electronic transition dipole moment, E_{ex} is the electronic transition energy. $\hbar\omega_i$ and $\hbar\omega_{LO}$ are the energies of the incident photon and the LO phonon, respectively. Γ is the homogeneous line width. $|g,n+j\rangle$ and $|g,j\rangle$ are the $(n+j)$th-order and jth-order LO phonon states in the electronic ground state, respectively. $|e,m\rangle$ is the mth-order LO phonon state in the electronic excited e state. k_B is Boltzmann's constant and T is the temperature. From this equation, the nth-order LO phonon mode intensity will become larger if $E_g\cong\hbar\omega_i-n\hbar\omega_{LO}$. The band gap of $Zn_{1-x}Mn_xO$ shifts to higher energy when Mn concentration increases, and it tends to be away from the frequency position of around 3500 cm^{-1}. Therefore, the intensity of sixth-order LO phonon mode decreases.

To investigate the dependence of RRS intensity on the band gap energy, temperature dependent RRS spectra of $Zn_{0.991}Mn_{0.009}O$ is shown in Fig. 4(a). At 10 K, the intensity of sixth-order LO phonon mode around 3500 cm^{-1} is the largest. However, when the temperature increases to 160 K, the seventh-order LO phonon mode around 4100 cm^{-1} becomes the largest in intensity. The behavior can be explained by considering the temperature dependence of the photoluminescence (PL). Fig. 4(b) shows the PL peak position of $Zn_{0.991}Mn_{0.009}O$ as a function of the temperature, and the curve can be fitted by considering the Bose–Einstein statistical factor for phonons [15]

$$E(T)=E(0)-\frac{2a_B}{\exp(\Theta/T)-1} \quad (3)$$

where $E(T)$ and $E(0)$ are the energies at T K and 0 K, respectively, a_B is the strength of the electron–phonon interaction, and Θ is associated with the mean frequency of the phonons. From Fig. 4(a) and (b), the shift of PL position results in the LO phonon line intensity variation. To summarize, multiple LO phonon scattering in RRS spectra can be explained by using the "cascade model" [16,17], the scattered photons will have energy $\hbar\omega\cong\hbar\omega_i-n\hbar\omega_{LO}$ or $\hbar\omega\cong\hbar\omega_i-n\hbar\omega_{E_{2(high)}}-n\hbar\omega_{LO}$. Moreover, by studying RRS spectra, we find that when the scattered photon energy is close to the band gap, the LO phonon intensity will be resonantly enhanced.

Fig. 5 shows the low temperature (10 K) PL spectra of $Zn_{0.997}Mn_{0.003}O$ analyzed by (σ_+) and (σ_-) circular polarization at magnetic field $B=0$ and $B=5$ T. At $B=0$, no difference was observed between two circular polarization. The D^0X (at 3.356 and 3.363 eV) and RRS (at 3.306 and 3.378 eV) intensities for (σ_+) and (σ_-) components are approximately the same. However, at $B=5$ T, a slight difference is observed between the two circular

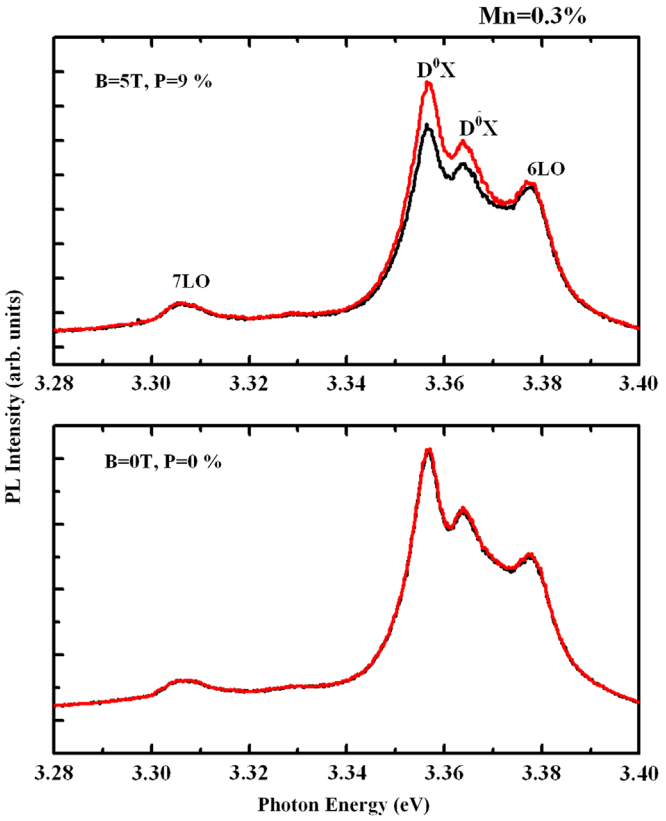

Fig. 5. Low temperature (10 K) PL spectra of $Zn_{0.997}Mn_{0.003}O$ for $B=0$ and $B=5$ T.

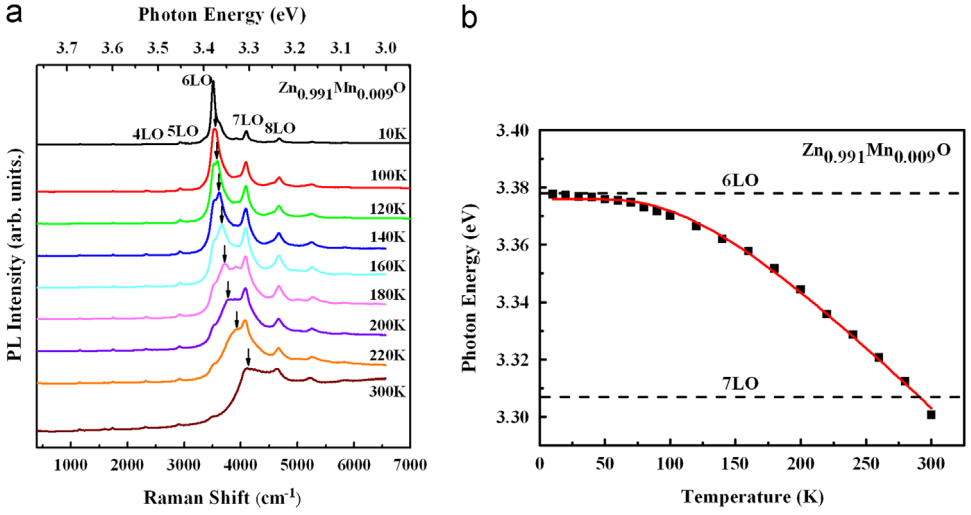

Fig. 4. (a) Resonant Raman scatterings of $Zn_{0.991}Mn_{0.009}O$ thin films with variable temperature, using the He–Cd laser ($\lambda=325$ nm). The arrows show the PL positions. (b) Temperature dependent photoluminescence (PL) position of $Zn_{0.991}Mn_{0.009}O$. The solid curve describes the fit of these data by using the Bose–Einstein statistical factor for phonons. The dashed lines represents the energy positions of the scattered photons with energy $\hbar\omega\cong\hbar\omega_i-n\hbar\omega_{LO}$, $n=6$ or 7.

polarization components of the D^0X. While the intensities of the two circular polarization components of the RRS remain the same. The degree of circular polarization can be defined as

$$P = \frac{I_{\sigma+} - I_{\sigma-}}{I_{\sigma+} + I_{\sigma-}} \quad (4)$$

where $I_{\sigma+}$ and $I_{\sigma-}$ are the intensities of the right and left circular polarization, respectively. For RRS, $P=0$ at $B=0$ and 5 T. Whereas, for D^0X emission, $P=0$ at 0 T and $P=9\%$ at 5 T. The non-zero circular polarization is due to the energy splitting of the two spin components of the D^0X, (electron $-1/2$ and hole $-3/2$) and (electron $+1/2$ and hole $+3/2$). Although, the energy separation is too small to be resolved, due the energy relaxation from the higher energy spin state to the lower energy spin state, $P=9\%$ is observed. The dependence of circular polarization on the magnetic field shows Brillouin-type para-magnetism. No hysteresis is observed. It implies that the $Zn_{0.997}Mn_{0.003}O$ exhibits paramagnetism due sp–d exchange interaction between conduction band s electrons/valence band p electron and d electrons of the Mn atoms.

4. Conclusion

We have grown $Zn_{1-x}Mn_xO$ ($x=0$–0.061) thin films by MBE. Transmittance measurement shows an increase of the band gap with the increasing Mn concentration. From RRS spectra, we observe LO phonon lines up to 5 and 11 order for ZnO and ZnMnO samples, respectively. From the temperature dependent RRS experiment, we find the intensities of these LO phonon lines are sensitive to the band gap position. Low temperature PL spectra of $Zn_{0.997}Mn_{0.003}O$ at magnetic field $B=0$ T and 5 T were investigated to calculate the degrees of circular polarization of $P=0\%$ and 9%, respectively.

Acknowledgments

This work was supported by the National Science Council and the Ministry of Education under the Grant numbers NSC100-2119-M-009-003 and MOE-ATU 101W961 respectively.

References

[1] T. Dietl, H. Ohno, F. Matsukara, J. Gilbert, D. Ferrand, Zener model description of ferromagnetism in zinc-blende magnetic semiconductors, Science 287 (2000) 1019.
[2] Parmanand Sharma, Amita Gupta, K.V. Rao, J. Owens, Renu Sharma, Rajeev Ahuja, J.M. Osorio Guillen, Börje Johansson, G.A. Gehring, Ferromagnetism above room temperature in bulk and transparent thin films of Mn-doped ZnO, Nature Materials 2 (2003) 673.
[3] Sejoon Lee, Youngmin Lee, Yoon Shon, Deuk Young Kim, Tae Won Kang, Tunneling transport properties for metal-oxide-semiconductor diode consisting of ferromagnetic ZnMnO nanocrystals, Applied Physics Letters 97 (2010) 182103.
[4] A.I. Savchuk, V.I. Fediv, G.I. Kleto, S.V. Krychun, S.A. Savchuk, Optical and magneto-optical properties of ZnMnO and ZnMnFeO single crystals and thin films, Physica Status Solidi A 204 (2007) 106.
[5] V.K. Sharma, B.K. Gupta, G.D. Varma, Optical and magnetic properties of (Zn,Mn)O nanostructures synthesized by CVD method, Crystal Research and Technology 46 (2011) 523.
[6] Yufeng Tian, Yongfeng Li, Mi He, Irwan Ade Putra, Haiyang Peng, Bin Yao, Siew Ann Cheong, Tom Wu, Bound magnetic polarons and p–d exchange interaction in ferromagnetic insulating Cu-doped ZnO, Applied Physics Letters 98 (2011) 162503.
[7] The-Long Phan, P. Zhang, D.S. Yang, N.X. Nghia, S.C. Yu, Local structure and paramagnetic properties of $Zn_{1-x}Mn_xO$, Journal of Applied Physics 110 (2011) 063912.
[8] Y.F. Chen, H.J. Ko, S.K. Hong, T. Yao, Layer-by-layer growth of ZnO epilayer on Al_2O_3 (0001) by using a MgO buffer layer, Applied Physics Letters 76 (2000) 559.
[9] C.A. Johnson, K.R. Kittilstved, T.C. Kaspar, T.C. Droubay, S.A. Chambers, G.M. Salley, D.R. Gamelin, Mid-gap electronic states in $Zn_{1-x}Mn_xO$, Physical Review B 82 (2010) 115202.
[10] T. Mizokawa, T. Nambu, A. Fujimori, T. Fukumura, M. Kawasaki, Electronic structure of the oxide-diluted magnetic semiconductor $Zn_{1-x}Mn_xO$, Physical Review B 65 (2002) 085209.
[11] R. Cusco, E. Alarcon-Llado, J. Ibanez, L. Artus, J. Jimenez, B. Wang, M.J. Callahan, Temperature dependence of Raman scattering in ZnO, Physical Review B 75 (2007) 165202.
[12] K.W. Boer, Survey of Semiconductor Physics: Electrons and Other Particles in Bulk Semiconductors, Van Nostrand Reinhold, New York, (1990), Chapter 28.
[13] J.F. Scott, T.C. Damen, W.T. Silfvast, R.C.C. Leite, L.E. Cheesman, Resonant raman scattering in zns and znse with the cadmium laser, Optics Communications 1 (1970) 397.
[14] M.C. Klein, F. Hache, D. Ricard, C. Flytzanis, Size dependence of electron–phonon coupling in semiconductor nanospheres: the case of CdSe, Physical Review B 42 (1990) 11123.
[15] P. Lautenschlager, M. Garriga, M. Cardona, Temperature dependence of the interband critical-point parameters of InP, Physical Review B 36 (1987) 4813.
[16] R.M. Martin, C.M. Varma, Cascade theory of inelastic scattering of light, Physical Review Letters 26 (1971) 1241.
[17] W.H. Sun, S.J. Chua, L.S. Wang, X.H. Zhang, Outgoing multiphonon resonant Raman scattering and luminescence in Be- and C-implanted GaN, Journal of Applied Physics 91 (2002) 4917.